Sixth International Symposium on Turbulence and Shear Flow Phenomena
Seoul, Korea, 22-24 June 2009

DIRECT NUMERICAL SIMULATIONS OF NON-ISOTHERMAL AND REACTING WALL-JETS

Z. Pouransari, G. Velter, D. Ahlman, G. Brethouwer and A.V. Johansson
Linné Flow Centre,
KTH Mechanics
SE-100 44 Stockholm, Sweden

ABSTRACT

Direct numerical simulations of plane compressible turbulent non-isothermal wall-jets are performed and compared to an isothermal jet. The study concerns a cold jet in a warm coflow and a warm jet in a cold coflow. The influence of the varying density on the flow and scalar mixing are studied. Although the domain length is somewhat limited in the simulations, the growth rate and the turbulence statistics indicate approximate self-similarity in the fully turbulent region. The use of van Driest scaling leads to a collapse of all mean velocity profiles in the near wall region. However, taking into account the varying density by using semi-local scaling of turbulent stresses and fluctuations does not completely eliminate differences between the statistics of the cold, isothermal and warm jet. The temperature and passive scalar dissipation time scales are similar in all cases.

A direct numerical simulation of a simple reaction in a turbulent plane wall-jet with a slight coflow is also performed. At the jet inlet the fuel is added whereas the oxidizer is added in the coflow. The reaction time scale is finite and of the same order as the mixing time scale. As the jet propagates downstream and becomes turbulent the reaction occurs mainly in the upper shear layer, but further downstream also in the inner layer due to the turbulent mixing.

INTRODUCTION

The plane wall-jet is an interesting case because the turbulence has different properties in the inner layer near the wall and the outer layer, and the flow can display self-similarity. Recently, Ahlman et al. (2007) studied an isothermal wall-jet by direct numerical simulations (DNS) and found similarities between the inner layer and a zero-pressure gradient boundary layer, and between the outer layer and a free shear layer. The flow statistics in the near-wall and outer region at different positions collapsed by applying inner and outer scaling respectively, which indicated self-similar development of the jet.

We have continued the work by Ahlman et al. (2007) and carried out fully compressible DNS of non-isothermal wall-jets: a cold jet in a warm coflow and a warm jet in a cold coflow (Ahlman et al., 2009). Previous studies have mainly examined compressible effects in relatively high Mach number flows, see e.g., Coleman et al. (1995). Studies of shear flows with significant density gradient and low Mach numbers are relatively scarce. In the present study, we therefore study non-isothermal turbulent wall-jets with low Mach numbers. The aim of the investigation is to study how the wall-jet development is influenced by the varying density. Properties of the non-isothermal jets are compared to results obtained in an isothermal jet. Proper scaling approaches in the respective inner and outer layers are investigated. The influence of the varying density on the mixing and transport of scalars is also studied, and the self-similarity of the velocity and scalar fields is evaluated.

We have also taken the next step and studied a simple reaction in turbulent wall-jet. The flow is compressible and a single step reaction between an oxidizer and a fuel species is solved. At the inlet fuel and oxidizer enter the domain separately in a non-premixed manner. The reaction is temperature independent and does not release heat. Since the flow is uncoupled from the reactions, the influence of turbulent mixing on the reactions can be studied in the absence of temperature effects.

DIRECT NUMERICAL SIMULATIONS

Figure 1 shows the flow geometry and coordinate system of the plane turbulent wall-jet. The inlet of the jet has a

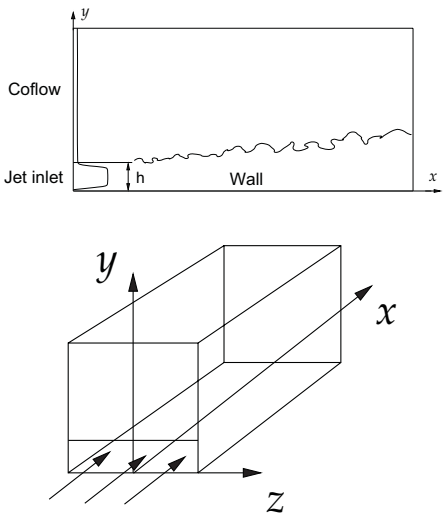

Figure 1: The plane wall-jet computational domain and coordinate system.

height h. The flow at the inlet is parallel to the wall. No-slip conditions are used for the velocity at the bottom wall and periodic boundary conditions are used in spanwise direction. A slight coflow is used to convect persistent vortices, which can develop above the jet flow in the initial period, out the domain. At the top of the domain there is a small flow into the domain to account for the entrainment.

governing equations

The governing equations in all jet simulations are the fully compressible Navier-Stokes equations

$$\frac{\partial \rho}{\partial t} + \frac{\partial \rho u_j}{\partial x_j} = 0 \quad (1)$$

$$\frac{\partial \rho u_i}{\partial t} + \frac{\partial \rho u_i u_j}{\partial x_j} = -\frac{\partial p}{\partial x_i} + \frac{\partial \tau_{ij}}{\partial x_j} \quad (2)$$

$$\frac{\partial \rho E}{\partial t} + \frac{\partial \rho E u_j}{\partial x_j} = \frac{\partial}{\partial x_j}\left(\lambda \frac{\partial T}{\partial x_j}\right) + \frac{\partial (u_i(\tau_{ij} - p\delta_{ij})}{\partial x_j} \quad (3)$$

where ρ is the mass density, u_j is the velocity vector, p is the pressure and $E = e + \frac{1}{2}u_i u_i$ is the total energy, being the sum of the internal energy e and kinetic energy. Fourier's law, where λ is the coefficient of thermal conductivity, is used to approximate the energy fluxes. The stress tensor is defined as

$$\tau_{ij} = \mu\left(\frac{\partial u_i}{\partial x_j} + \frac{\partial u_j}{\partial x_i}\right) - \frac{2}{3}\mu\delta_{ij}\frac{\partial u_k}{\partial x_k} \quad (4)$$

where μ is the dynamic viscosity.

The fluid is assumed to be calorically perfect and to obey the ideal gas law

$$e = c_v T \quad (5)$$

$$p = \rho R T \quad (6)$$

and a ratio of specific heats of $\gamma = c_p/c_v = 1.4$ is used. To account for the substantial variations in density and temperature a temperature dependent viscosity is used in the non-isothermal cases. The viscosity is determined through Sutherland's law

$$\frac{\mu}{\mu_j} = \left(\frac{T}{T_j}\right)^{3/2}\frac{T_j + S_0}{T + S_0} \quad (7)$$

where T is the local temperature, T_j the jet center temperature at the inlet and S_0 a reference coefficient.

Non-isothermal wall-jet simulations

Two DNS of non-isothermal wall-jets have been carried out: a cold jet in a warm coflow with an ambient to jet density ratio of $\rho_a/\rho_j = 0.4$, and a warm jet in a cold coflow with a density ratio of $\rho_a/\rho_j = 1.7$. The coflow and wall temperature are equal. In addition a transport equation for a passive scalar is solved. The Schmidt number $Sc = 1.0$ and there is no scalar flux through the wall. At the jet inlet, the Reynolds number $Re = U_j h/\nu_j = 2000$, where ν_j and U_j are the kinematic viscosity and velocity at the inlet jet center respectively. The Mach number $M = U_j/c = 0.5$. These two parameters are equal in all DNS, including the isothermal DNS by Ahlman et al. (2007). A simulation of a cold jet with $Re = 7000$ has also been carried out to assess the influence of the Reynolds number.

A fully compressible code with sixth-order compact finite difference scheme for the spatial discretisation is used. The spatial resolution in terms of wall units is comparable with many other DNS of turbulent channel flows. The goal of the investigation is to study turbulent wall-jets, hence disturbances are applied at the jet inlet to facilitate a fast and efficient transition to turbulence. Table 1 shows the inlet density ratios and the reference name for each case, and table 2 shows the box dimensions and resolutions. More details on the simulations can be found in Ahlman et al. (2007, 2009).

Table 1: Simulation cases.

Jet	Case	Re	ρ_a/ρ_j	Line style
Isothermal	I2	2000	1.0	———
Cold	C2	2000	0.4	– · –
Warm	W2	2000	1.7	– – –
Cold	C7	7000	0.4	–×–

Table 2: Simulation parameters. L_x, L_y, L_z and N_x, N_y, N_z are the streamwise, wall-normal and spanwise box dimensions in terms of inlet jet height h and grid resolution, respectively.

Case	$L_x \times L_y \times L_z$	$N_x \times N_y \times N_z$
I2	$47 \times 18 \times 9.6$	$384 \times 192 \times 128$
C2	$35 \times 17 \times 7.2$	$384 \times 192 \times 160$
W2	$28 \times 14 \times 7.2$	$448 \times 256 \times 160$
C7	$30 \times 16 \times 8.0$	$256 \times 192 \times 128$

Reacting wall-jet simulation

A DNS of a reaction in an isothermal turbulent wall-jet has also been carried out. The flow configuration and simulation method are the same as in the non-isothermal wall jet simulations. We consider a simple irreversible reaction between an oxidant species O and a fuel species F forming a product P

$$O + F \longrightarrow P. \quad (8)$$

The reaction mass rate is formulated as

$$\dot{\omega}_f = \dot{\omega}_o = \dot{\omega} = k_r \rho^2 \theta_o \theta_f \quad (9)$$

where k_r is the reaction rate coefficient. The reaction is temperature independent and does not release heat. Apart from the oxidizer and fuel a passive scalar equation is solved. The passive scalar is used to compare statistics between reacting and non-reacting species. Conservation of the species masses are governed by

$$\frac{\partial \rho\theta_o}{\partial t} + \frac{\partial}{\partial x_j}(\rho\theta_o u_j) = \frac{\partial}{\partial x_j}\left(\rho\mathcal{D}\frac{\partial \theta_o}{\partial x_j}\right) - \dot{\omega} \quad (10)$$

$$\frac{\partial \rho\theta_f}{\partial t} + \frac{\partial}{\partial x_j}\left(\rho\theta_f u_j\right) = \frac{\partial}{\partial x_j}\left(\rho\mathcal{D}\frac{\partial \theta_f}{\partial x_j}\right) - \dot{\omega} \quad (11)$$

$$\frac{\partial \rho\theta}{\partial t} + \frac{\partial}{\partial x_j}(\rho\theta u_j) = \frac{\partial}{\partial x_j}\left(\rho\mathcal{D}\frac{\partial \theta}{\partial x_j}\right) \quad (12)$$

where θ_o, θ_f and θ are the mass fractions of the oxidizer, fuel and passive scalar respectively. The diffusion coefficient $\mathcal{D}$ is equal for all scalars.

The inlet Reynolds and Mach numbers of the simulation are 2000 and 0.5, respectively. The computational domain size is $(L_x = 22h) \times (L_y = 14h) \times (L_z = 3.6h)$ and the resolution is $(N_x = 256) \times (N_y = 192) \times (N_z = 80)$ which corresponds to that in the other simulations.

To specify the reaction rate Damköhler number $Da = hk_r\rho_j/U_j = 3$ is used. The reaction timescale is this finite and is of the same order as the convection time scale. The fuel and oxidizer on non-premixed; at the jet inlet $\Theta_{f,j} = 1$, while in the coflow $\Theta_{o,c} = 0.5$.

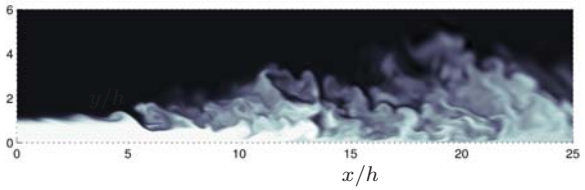

Figure 2: Snapshot of the passive scalar concentration in the warm jet.

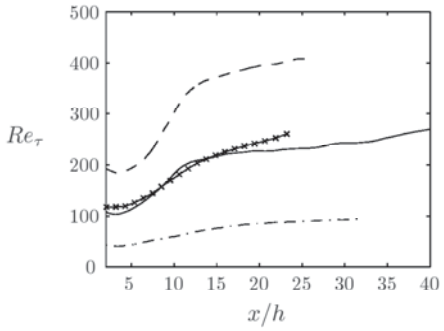

Figure 3: Downstream development of the friction Reynolds number $Re_\tau = u_\tau y_{1/2}/\nu_w$.

RESULTS

Non-isothermal wall-jet simulations

Figure 2 presents a snapshot of the passive scalar field in the warm jet DNS. We can see the growth of the instabilities and the transition process. At about $x/h = 15$ the flow is fully turbulent.

Although the inlet Reynolds number is the same in cases C2, I2 and W2 the friction Reynolds number

$$Re_\tau = \frac{u_\tau \delta}{\nu_w} = \frac{\delta}{\nu_w^{1/2}} \sqrt{\left(\frac{dU}{dy}\right)_{y=0}}, \tag{13}$$

where ν_w is the viscosity at the wall, is different. This is shown in figure 3. In the fully turbulent region, Re_τ in the warm jet is about 4.5 times higher than in the cold jet at $Re = 2000$. Consequently, in the warm jet the turbulence structures are smaller and the scale separation between the inner and outer shear layer is larger than in the cold jet. The difference in Re_τ is related to the temperature dependence of the viscosity at wall temperature. In the warm jet ν_w is low near the relatively cold wall, whereas in the cold jet ν_w is high near the relatively warm wall, which results in high and low Re_τ respectively. The higher inlet Reynolds number in case C7 leads to a Re_τ about equal to that in case I2.

Structural compressibility effects on turbulence are not expected when the density fluctuations are small. The density fluctuations scaled by the mean density in the non-isothermal jets are approximately at the level where compressible effects could become noticeable, but can still be considered small.

The mean streamwise velocity profiles of the wall-jets in conventional wall variable scaling do not collapse outside the viscous sublayer. This has also been observed to occur in compressible boundary layers or channel flows with significant temperature variations near the wall. Alternative scaling approaches have been developed which take into account the mean density variation. One of these is the van Driest transformation defined as

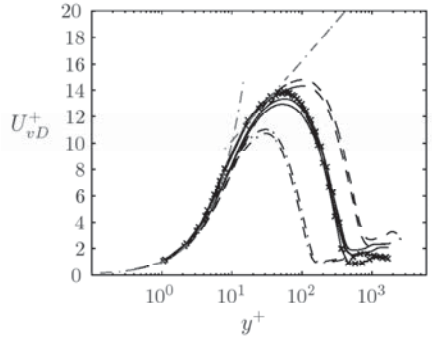

Figure 4: Mean streamwise velocity using the van Driest transformation. Profiles at $x/h = 20$ and $x/h = 25$ for cases C2, I2 and W2. Profiles at $x/h = 17$ and $x/h = 22$ for case C7. The line styles are defined in table1. Viscous, $U^+ = y^+$, and inertial sublayer, $U^+ = \log(y^+)/0.38 + 4.1$ (the straight dash-dotted line) profiles added.

$$U^+_{vD} = \int_0^{U^+} (\bar\rho/\bar\rho_w)^{1/2}\, dU^+, \tag{14}$$

where $\bar\rho_w$ is the mean density at the wall. Using the van Driest transformation, the mean velocity profiles of compressible flows and incompressible flows are similar (see e.g., Coleman et al., 1995). Van Driest transformed wall-jet profiles are shown in figure 4. Here, $y^+ = y u_\tau/\nu_w$. As a result of the transformation the profiles are slightly more similar than in conventional wall scaling, but they still don't collapse outside the buffer layer. In the warm jet, which has the highest Re_τ, a logarithmic region in accordance with the incompressible inertial sublayer, starts to appear.

Another approach to account for density variations is the semi-local scaling proposed by Huang et al. (1995). In this scaling the wall variables are based on the local mean density and viscosity, and their relation to the conventional wall units becomes as a result

$$u^*_\tau = \sqrt{\frac{\tau_w}{\bar\rho}} = \sqrt{\frac{\bar\rho_w}{\bar\rho}}\, u_\tau \tag{15}$$

$$l^* = \frac{(\bar\mu/\bar\rho)}{u^*_\tau} = \frac{(\bar\mu/\bar\mu_w)}{\bar\rho/\bar\rho_w} l^+, \tag{16}$$

where $u_\tau = \sqrt{\tau_w/\bar\rho_w}$ and $l^+ = \bar\nu_w/u_\tau$ are the conventional friction velocity and length scales, and wall conditions are denoted by a subscript w. We define $y^* = y/l^*$. However, figure 5 shows that this scaling does not lead to a collapse of the streamwise velocity fluctuation profiles of the four DNS, which indicates that the mean density variations affect the scaling properties of the turbulence.

To evaluate self-similarity in the outer region, profiles of the streamwise velocity fluctuations of the four jets are shown in figure 6 in terms of the isothermal outer scaling. The velocity half-width is the distance from the wall where the mean velocity is equal to half the mean excess value, i.e. $\tilde U(x, y_{1/2}(x)) = \frac{1}{2}(\tilde U_m(x) - \tilde U_c)$, where $\tilde U_m(x)$ is the maximum mean velocity and $\tilde U_c$ the coflow velocity. The outer scaling leads to a collapse of the profiles of cases I2, W2 and C7 whereas the profiles of case C2 differ, probably because of the low Re_τ. The streamwise velocity fluctuation profiles of the warm and isothermal jet are quite similar. In

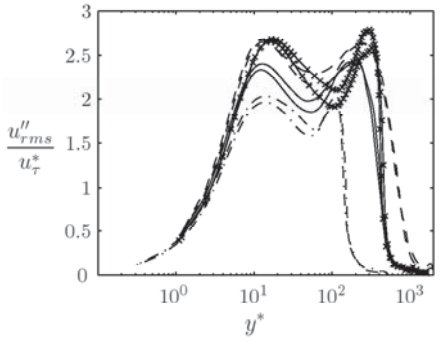

Figure 5: Streamwise fluctuation intensity using semi-local normalization. Profiles at $x/h = 20$ and $x/h = 25$ for cases C2, I2 and W2. Profiles at $x/h = 17$ and $x/h = 22$ for case C7.

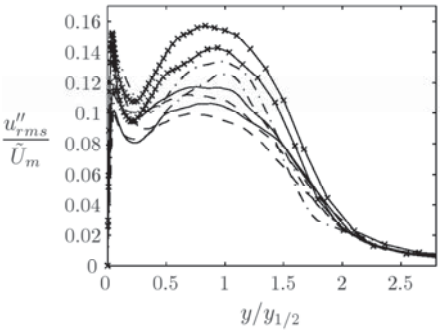

Figure 6: Streamwise fluctuation intensity in outer scaling. Profiles at $x/h = 20$ and $x/h = 25$ for cases C2, I2 and W2. Profiles at $x/h = 17$ and $x/h = 22$ for case C7.

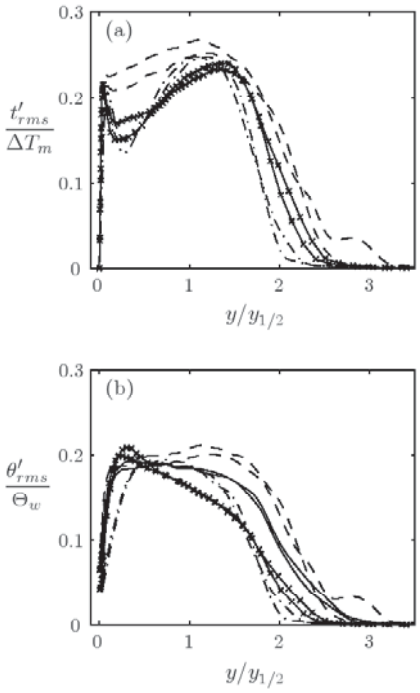

Figure 7: Temperature (a) and passive scalar (b) fluctuation intensities. Profiles at $x/h = 20$ and $x/h = 25$ for cases C2, I2 and W2. Profiles at $x/h = 17$ and $x/h = 22$ for case C7.

contrast, the maximum scaled streamwise fluctuation intensity of the two cold jets in the outer layer is higher than in the isothermal and warm jet which shows the relative high turbulence intensity in the two former cases. Other profiles of the mean and fluctuating velocities are significantly different in the three DNS as well but the differences between Favre and Reynolds averaged statistics are small. The compressible effects are thus mainly a result of the mean density variations. The fairly good collapse of the scaled velocity and turbulence profiles that we have observed at different downstream positions indicates an approach to self-similarity. Compressibility effects are seen in the density and temperature fluctuations but are small despite the significant density difference between the jet and coflow.

In figure 7 the fluctuation intensity of the temperature and passive scalar are presented. The fluctuations are normalized by the maximum temperature and scalar difference, $\Delta\Theta_m = \Theta_w \equiv \bar{\Theta}_w$, and $\Delta T_m = \max(|\bar{T}_w - \bar{T}|)$. Passive scalar fluctuations are in the cold jet at Re=7000 near the wall larger than in the outer layer where the fluctuations further decrease in intensity. In contrast, the passive scalar fluctuations are of comparable magnitude in the inner and outer layer in the other jets at $Re = 2000$. In the warm jet the intensity even increases slightly for $y > y_{1/2}$. Scaled with ΔT_m and Θ_w, the temperature and passive scalar fluctuations respectively have a similar intensity in the inner region in all simulations, with the exception of case C2 which shows small passive scalar fluctuations there. In the outer layer, the intensity of the passive scalar fluctuations is lower than of the temperature using outer scaling, in particular in case C7. The maximum intensity of the temperature fluctuation in the outer layer scales approximately with the maximum temperature difference. Near the wall, the fluctuations show distinct peaks in the two cold jet cases but not in the warm jet. The difference between the inner and outer layer is thus less pronounced in the warm jet than in the cold jets. This is somewhat counter-intuitive because an increased scale separation in most cases acts to pronounce differences between the inner and outer regions. The maximum value of the normalized passive scalar flux in the outer layer appears to increase with increasing Re_τ. In the inner layer, the magnitude of the normalized wall-normal temperature flux is larger in case C7 than in the warm jet but in the outer layer it is comparable.

The ratio of the mechanical to passive scalar time scale and the corresponding temperature to passive scalar time scale ratio are presented in figure 8. In the outer layer, no clear effect of the density differences is perceivable in the mechanical to passive scalar time scale ratio. The time scale ratio is relatively constant throughout most of the wall-jet, with exception for the inner region. For the passive scalar the time scale ratio shows even less variation in the outer region. The ratio of the temperature and passive scalar time scale is less than one indicating a more intense dissipation of temperature fluctuations than of passive scalar fluctuations.

We have also computed growth rates, turbulent heat and passive scalar fluxes, and temperature and passive scalar dissipation rates. See Ahlman et al. (2009) for more results.

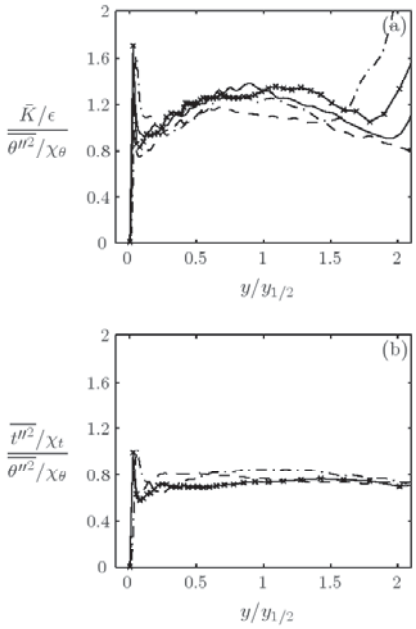

Figure 8: Mechanical to scalar (a) and temperature to passive scalar (b) time scale ratio.

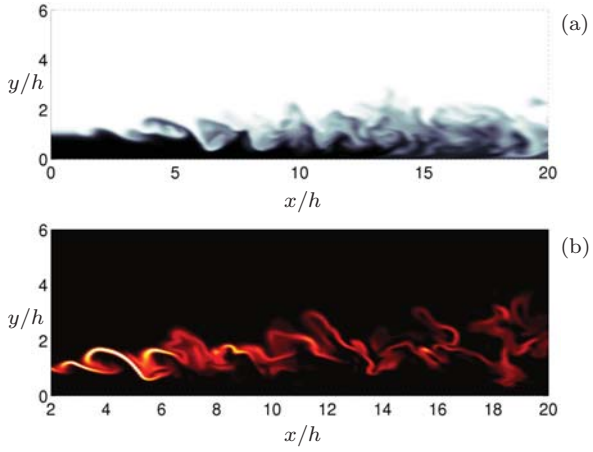

Figure 9: Snapshots of the fuel concentration (a) and reaction rate $\dot{\omega}$ (b). A light colour in (b) corresponds to a high reaction rate.

Reacting wall-jet simulation

In figure 9(a) a snapshot of the fuel mass fraction is shown. Cross stream profiles of the mean scalar concentrations are shown in figure 10. whereas the oxidizer fraction is less affected. We see a clear difference between the mean passive scalar and fuel concentration profiles. A significant fraction of the fuel is thus consumed by the reaction The reaction starts immediately after the inlet and occurs in a sheet like structure as shown by figure 9 (b). We see that the reaction mainly occurs in the free shear layer where the oxidizer and the fuel mix. This is confirmed by figure 11 showing that the maximum mean reaction rate takes place at the jet half-width position $y_{1/2}$. However, the fuel and oxidizer also react near the wall.

Cross stream profiles of the wall-normal scalar fluxes are presented in figure 12 using outer layer normalization. The flux of the non-reacting scalar compare well with the previous non-reacting simulation results but the wall-normal flux of the fuel is smaller than the passive scalar flux in the outer layer.

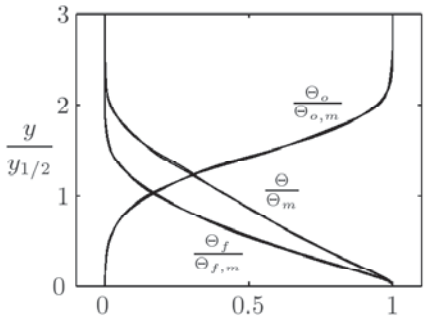

Figure 10: Mean scalar profiles at $x/h = 17$ and 20 using outer layer normalization.

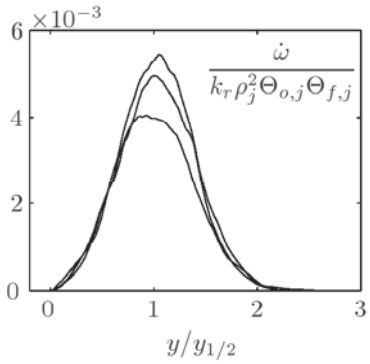

Figure 11: Inlet normalized mass reaction rate at $x/h = 15, 17, 20$.

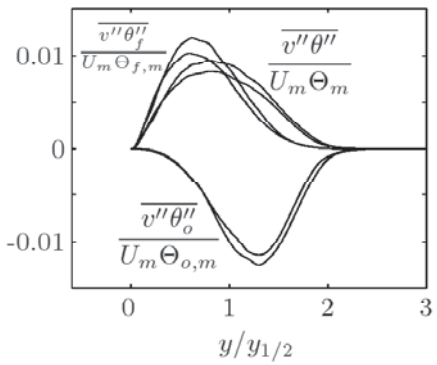

Figure 12: Wall-normal fluxes of the reacting and non-reacting scalars at $x/h = 17$ & 20.

CONCLUSIONS

Direct numerical simulations of a warm wall-jet in a cold environment and a cold jet in a warm environment have been carried out (Ahlman et al., 2009). The inlet Reynolds number and Mach number are the same as in a previously performed isothermal wall-jet simulation (Ahlman et al., 2007). In addition, a cold jet at a higher Reynolds number has been simulated.

Statistics of the jet development, turbulence and mixing are presented and the results are compared to statistics of the isothermal jet. Due to the varying viscosity the friction Reynolds numbers are different. Correspondingly, in the warm jet smaller turbulence structures are present and the scale separation between the inner and outer shear layer is larger than in the cold jet at the same inlet Reynolds number. As a result of the density variation, conventional wall scaling fails to collapse the non-isothermal and isothermal jets outside the viscous sublayer. Semi-local scaling is not capable of collapsing the near wall streamwise fluctuations intensities. The profiles of the streamwise velocity fluctuations in outer scaling do not collapse either in the outer layer. The normalized turbulence statistics thus appear to be influenced by mean density variations. On the other hand, the differences between Favre and Reynolds averages are small. The compressible effects are thus mainly a result of the mean density variations. The mechanical to scalar time scale behaviour is approximately equal in the four jets. The ratio of the temperature to passive scalar time scale is less than one indicating a smaller temperature time scale and hence a more intense dissipation of temperature fluctuations.

A reacting turbulent plane wall-jet was also studied by direct numerical simulations. A single reaction between a fuel and an oxidizer species without heat release was used. The reaction and convection time scale were specified to be of the same order. The snapshots of the species and the reaction term showed that the reaction mainly occurs in the upper shear layer in thin highly convoluted reaction zones. The reaction rate term has a maximum near the jet half width $y_{1/2}$, but the fuel and oxidizer react also near the wall, although to a lesser extent.

REFERENCES

Ahlman, D., Brethouwer, G. and Johansson, A. V., 2007, "Direct numerical simulation of a plane turbulent wall-jet including scalar mixing", *Phys. Fluids*, Vol. 19, 065102.

Ahlman, D., Velter, G., Brethouwer, G. and Johansson, A. V., 2009, "Direct numerical simulation of non-isothermal turbulent wall-jets' *Phys. Fluids*, Vol. 21, 035101.

Coleman, G. N., Kim, J. and Moser, R. D., 1995, "A numerical study of turbulent supersonic isothermal-wall channel flow", *J. Fluid Mech.*, Vol. 305, pp. 159-183.

Huang, P. G., Coleman, G. N. and Bradshaw, P., 1995, "Compressible turbulent channel flows: DNS results and modelling", *J. Fluid Mech.*, Vol. 305, pp. 185-218.